Advanced Composite Materials
Publication details, including instructions for authors and subscription information:
http://www.tandfonline.com/loi/tacm20

Scanning electron microscopy study of failure in glass-sealed SiC/SiC-based composite (NUSK-CMC) creep tested at 1100 and 1200°C in air

I. J. Davies , T. Ogasawara & T. Ishikawa
Version of record first published: 02 Apr 2012.

To cite this article: I. J. Davies , T. Ogasawara & T. Ishikawa (2001): Scanning electron microscopy study of failure in glass-sealed SiC/SiC-based composite (NUSK-CMC) creep tested at 1100 and 1200°C in air , Advanced Composite Materials, 10:4, 357-367

To link to this article: http://dx.doi.org/10.1163/156855101753415382

Adv. Composite Mater., Vol. 10, No. 4, pp. 357–367 (2001)

Scanning electron microscopy study of failure in glass-sealed SiC/SiC-based composite (NUSK-CMC) creep tested at 1100 and 1200°C in air

I. J. DAVIES [1,*], T. OGASAWARA [2] and T. ISHIKAWA [2]

[1] *Advanced Fibro-Science, Kyoto Institute of Technology, Matsugasaki, Sakyo-ku, Kyoto 606-8585, Japan*

[2] *Structures Division, National Aerospace Laboratory, Mitaka City, Tokyo 181-0015, Japan*

Abstract—A scanning electron microscopy investigation was carried out for glass-sealed 3D woven SiC/SiC-based composite that had failed following creep testing at 1100 and 1200°C in air. It was shown that most specimens failed due to oxygen ingression into the composite that initiated at the specimen corner. The main path for oxygen movement with specimens was found to be along z fibre bundles. A simple analysis of the glass evaporation rate showed higher evaporation rates to always exist at the specimen corners and this could help to explain initiation of long-term creep failure.

Keywords: SiC/SiC composite; glass-sealed SiC/SiC; SEM investigation; creep testing; glass evaporation.

1. INTRODUCTION

Although ceramic matrix composites (CMCs) exhibit potential for many applications as high temperature structural materials in the aerospace and space fields, a continuing problem is that of oxidation of the fibre/matrix interface [1], which tends to suppress crack deflection at the fibre/matrix interface and changes the mode of failure from pseudo-ductile to brittle. One method of overcoming this problem has been to coat [2] or impregnate [3] the CMC with an oxidation barrier material in order to reduce oxygen diffusion into the material and hence provide longer operational lifetimes at elevated temperatures (e.g. >1000°C) in an oxidising atmosphere.

One such CMC with an oxidation protection system has been developed in collaboration between the National Aerospace Laboratory (Japan), Ube Industries

*To whom correspondence should be addressed. E-mail: davies@ipc.kit.ac.jp

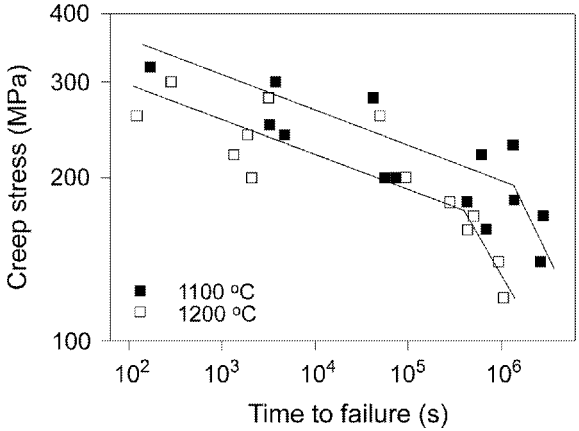

Figure 1. Time to failure as a function of creep stress for specimens tested at 1100 and 1200°C in air (adapted from [9]).

Ltd., Shikibo Ltd., and Kawasaki Heavy Industries Ltd., and has been named 'NUSK-CMC'. This composite, based on the SiC/SiC system, has been the subject of previous investigation by the authors [4–9]. Recent work has concentrated on the creep behaviour when tested at 1100 to 1300°C in air [8, 9]. For example, the effect of creep stress on time to failure for glass-sealed specimens tested at 1100 and 1200°C in air [8, 9] has been presented in Fig. 1. The main features of the data are the 'knee-points' at 1×10^6 s (1100°C) and $3–4 \times 10^5$ s (1200°C) and coincident with significant crystallisation of the glass sealant [9]. Increased crystallisation was believed to result in failure due to increased viscosity and/or volume contraction of the glass sealant [9], thus leading to accelerated specimen failure. Other factors such as specimen geometry are also believed to play a role in accelerated creep failure for this composite.

The present investigation is divided into two sections, the first of which summarises results from a scanning electron microscopy (SEM) investigation of fracture surfaces following creep testing at 1100 and 1200°C in air. The latter section provides an analysis to account for the effect of specimen geometry on accelerated specimen failure due to differential glass evaporation.

2. EXPERIMENTAL PROCEDURE

The composite system under investigation has been described in detail elsewhere, together with details of the creep testing apparatus [8, 9]. Essentially, the composite comprised surface-modified Tyranno® LoxM Si-Ti-C-O fibres woven into an orthogonal 3D architecture with fibre volume fractions of approximately 0.19, 0.19, and 0.02 in the x, y, and z directions, respectively. Matrix consolidation was achieved from the repeated impregnation and pyrolysis of a polymer similar to polytitanocarbosilane. Following machining to the required test dimensions, specimens

were repeatedly impregnated with a proprietary SiO_2-Na_2O-based glass in order to fill residual open porosity and seal the specimen surface. Following creep testing at 1100 and 1200°C in air, specimen fracture surfaces from a total of 17 specimens were examined using SEM (JSM-6300F, JEOL, Japan).

3. RESULTS AND DISCUSSION

3.1. Summary of the SEM investigation

Due to constraints of space, in this section, conclusions made from analysis of 17 specimens have been illustrated through a limited number of specimens. A fracture surface exhibiting characteristics typical of most specimens has been presented in Fig. 2a whilst accompanying fibre bundle positions, approximate oxygen path within the specimen (*black arrows*), and boundary between oxidised and unoxidised regions (*broken line*) have been included in Fig. 2b. Oxygen

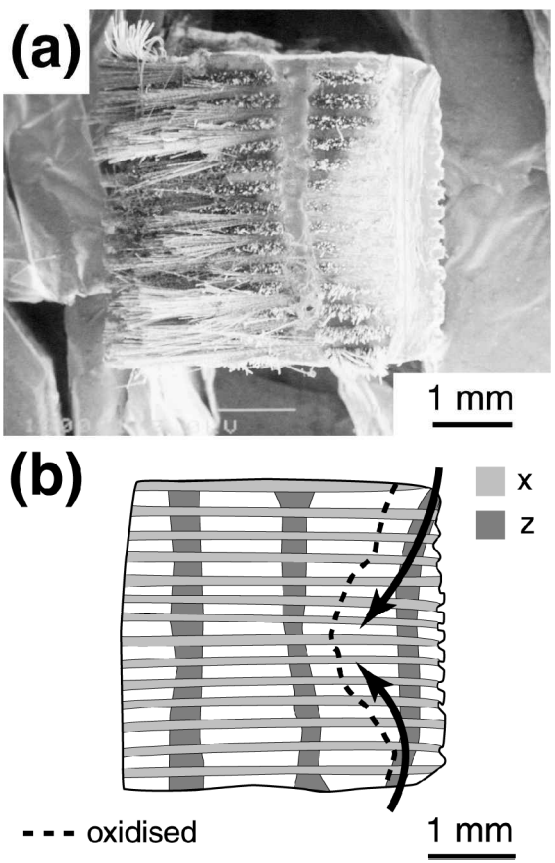

Figure 2. General view of a specimen that failed after 120 s under a stress of 260 MPa at 1200°C in air.

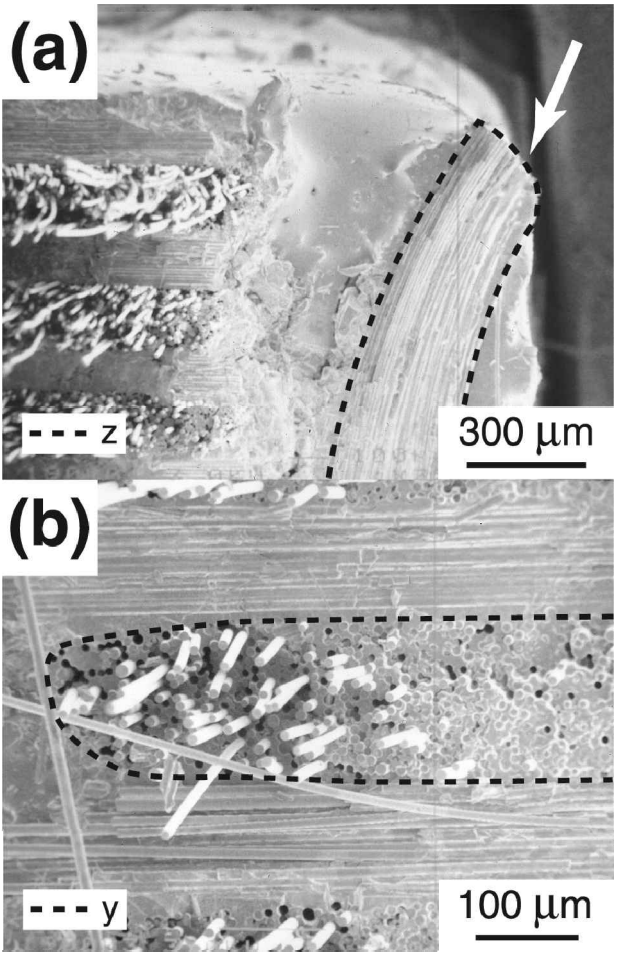

Figure 3. Detailed view of a specimen that failed after 120 s under a stress of 260 MPa at 1200°C in air.

ingression into the specimen appeared to initiate at both ends of the *z* fibre bundle at the specimen corner (Fig. 3a) and then moved relatively quickly along the *z* fibre bundle before proceeding along the *x* and *y* fibre bundles. Indeed, it was noted generally that the *z* fibre bundles were the preferred oxygen route within specimens, perhaps as a result of the continuous carbon layer present at the fibre/matrix interface. The symmetrical convex shape of the oxidised region suggests that oxygen ingression occurred at similar times at both ends of the *z* fibre bundle. Combined with the fact that the present specimen failed after only 120 s of creep loading, it was concluded that both ends of the *z* fibre bundle at the specimen corners had not been sufficiently coated/sealed with the glass protective layer.

Despite the specimen in Fig. 2 failing after a relatively short creep loading time, it was in fact the case that nearly all specimens (15 out of 17) showed initial oxygen

ingression at their corners and this was attributed to several factors: (i) reduced initial glass layer thickness at the corners, (ii) selective evaporation of Na atoms and resulting crystallisation of the glass layer having a greater effect at the corners, and (iii) increased glass evaporation at the corners due to geometrical effects. The first factor was generally applicable to specimens with creep lifetimes on the order of several minutes, including that shown in Fig. 2. The second factor was found to apply particularly to specimens with extended creep lifetimes and has been covered in detail elsewhere [9]. The contribution from the third factor has been analysed in the second section of this report.

Figure 3b illustrates a single y direction fibre bundle in which the left side is seen to exhibit significant fibre pullout (typically 100 μm) whilst the right side shows negligible pullout. It we consider the effect of fibre/matrix interface shear strength, τ, on fibre pullout length [4–6], it can reasonably be assumed that the left side of the fibre bundle comprises a low τ region whilst the right side represents a high τ region. The reason for this difference is that the fibre bundle in question was positioned at the boundary of the oxidised and unoxidised regions. Therefore, the oxidised region (right side) showed negligible fibre pullout, as τ had increased (due to oxidation of the interface) to such an extent that microcrack deflection at the fibre/matrix interface no longer came into play [10] whereas τ for the relatively unoxidised region (left side) was still low enough to allow microcrack deflection and fibre pullout over a considerable distance. It would thus appear that significant differences in the degree of oxidation, and hence τ, may be present within individual fibre bundles on a length scale of 100–200 μm.

A micrograph showing the corner of a failed specimen has been presented in Fig. 4a whilst positions of the respective fibre bundles and glass sealant have been included in Fig. 4b. The average glass thickness at the specimen surface in Fig. 4a is noted to be on the order of 50 μm and this was typical for all specimens investigated. Although the glass sealant thickness is seen to decrease to almost zero at the specimen corner, initial oxygen ingression into this specimen was not thought to have occurred at this position. Instead, when viewed at a lower magnification (Fig. 5), it would seem that oxygen ingression occurred at the middle left side (Fig. 5b), despite the glass thickness being approximately 50 μm at this position. Instead, consideration of the forces upon loading suggested a stress concentration to be present at the point of oxygen ingression due to the presence of a foreign object/defect observed within the specimen.

Overall, it was concluded that almost every specimen failed due to oxygen ingression at the specimen corner. Failure at short stress lifetimes (order of a few minutes) was attributed to incomplete coating/sealing of z bundles at the specimen surface whereas failure at the longest stress lifetimes was believed to be largely dependent on selective loss of Na and crystallisation of the glass sealant [9]. It will be shown in the next section that evaporation loss for the glass sealant is increased at the specimen corners due to a geometrical effect.

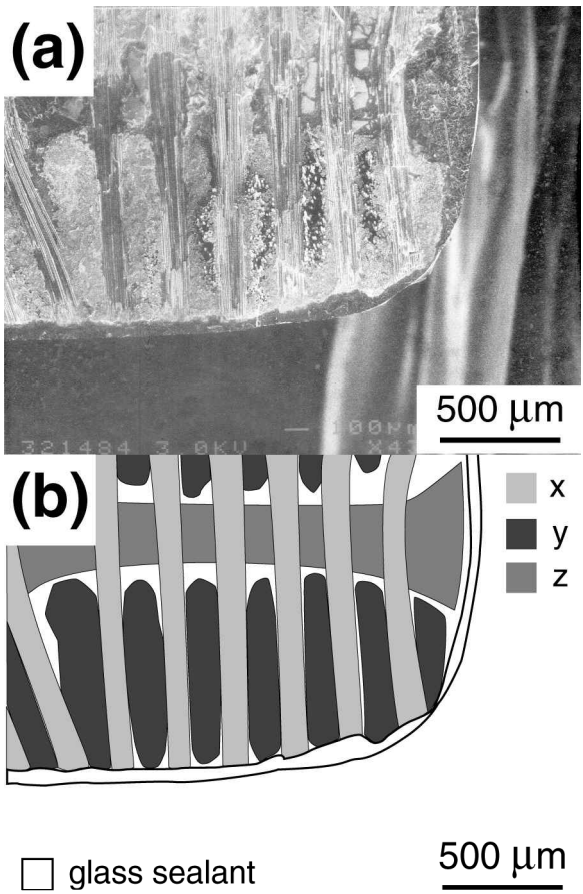

Figure 4. Micrograph showing the corner of a specimen that failed after 9.3×10^5 s under a stress of 140 MPa at 1200°C in air.

3.2. Analysis of glass evaporation at a curved surface

The aim of this section is to show that a significant contributory factor to oxygen ingression occurring at specimen corner edges may be to that of differences in the glass evaporation rate between the specimen corner edges and sides.

If we consider a sphere of radius, R, surrounded by a glass layer of thickness, t, then, from the standpoint of geometrical effects, the initial evaporation rate, E, from a point in the glass layer at a distance, r, from the sphere centre may be reasonably assumed to be a function only of x for any given direction, ϕ and θ, as shown in Fig. 6. From simple geometry, x may be given in terms of r, R, t, and ϕ by:

$$x = r\cos\phi + \sqrt{(R+t)^2 - r^2\sin^2\phi}. \tag{1}$$

The initial evaporation rate, $E(x)$, at any given point, for fixed ϕ and θ, will be a decreasing function of x and would be expected to decrease disproportionately

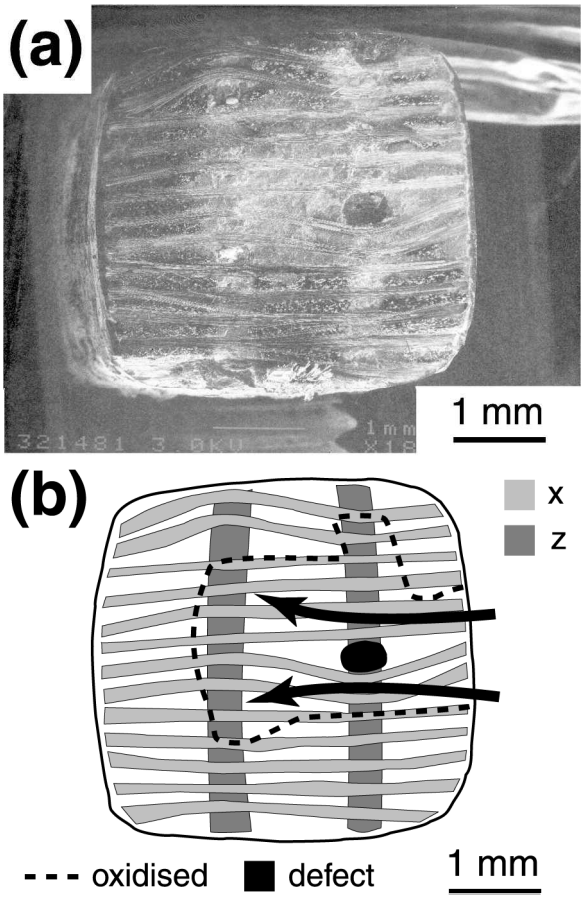

Figure 5. General view of a specimen that failed after 9.3×10^5 s under a stress of 140 MPa at 1200°C in air.

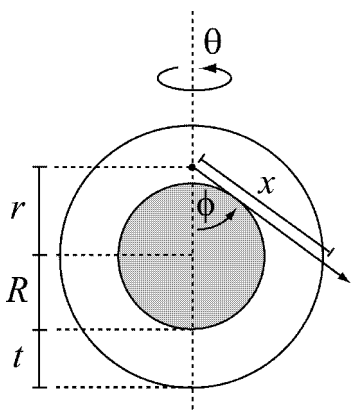

Figure 6. Schematic diagram showing the geometry assumed when calculating evaporation rate for a glass-coated sphere.

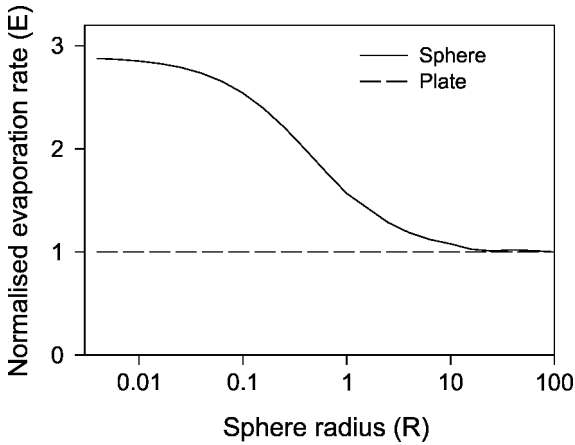

Figure 7. Effect of sphere radius on evaporation rate for a glass-coated sphere.

with increasing x. The evaporation rate would also be expected to increase with temperature, T, and decrease with activation energy, Q. A suitable function for $E(x)$ is that of:

$$E(x) = A\mathrm{e}^{-\left(\frac{Qx}{kT}\right)}, \tag{2}$$

where A is a constant and k is the Boltzmann constant. The total evaporation rate from a given point requires integration over the valid range of ϕ and θ, i.e.

$$E(r,\phi,\theta) = A\int_0^{2\pi}\int_{\phi_{\min}}^{\pi} \mathrm{e}^{-\left[\frac{Q(r\cos\phi+\sqrt{(R+t)^2-r^2\sin^2\phi)}}{kT}\right]}\partial\phi\partial\theta \quad \text{with } \phi_{\min} = \sin^{-1}\left(\frac{R}{r}\right). \tag{3}$$

The next step is to integrate $E(r,\phi,\theta)$ over the entire glass layer and this is achieved through transformation of the integration to the spherical coordinates, r, ω, and ψ, i.e.

$$E' = \int_0^{2\pi}\int_0^{\pi}\int_R^{R+t} r^2\sin\omega\left[A\int_0^{2\pi}\int_{\phi_{\min}}^{\pi} \mathrm{e}^{-\left[\frac{Q(r\cos\phi+\sqrt{(R+t)^2-r^2\sin^2\phi)}}{kT}\right]}\partial\phi\partial\theta\right]\partial r\partial\omega\partial\psi. \tag{4}$$

Simplifying this expression and normalising the evaporation rate with respect to the sphere surface area results in the following normalised initial evaporation rate:

$$E = \frac{2\pi A}{R^2}\int_R^{R+t} r^2\int_{\phi_{\min}}^{\pi} \mathrm{e}^{-\left[\frac{Q(r\cos\phi+\sqrt{(R+t)^2-r^2\sin^2\phi)}}{kT}\right]}\partial\phi\partial r. \tag{5}$$

This expression may not be further reduced analytically and thus must be solved numerically. In order to simplify calculations, all terms were set to unity apart from those specifically being varied in the following discussion. In addition, E was further normalised with respect to the case of a flat plate (i.e. $R \to \infty$).

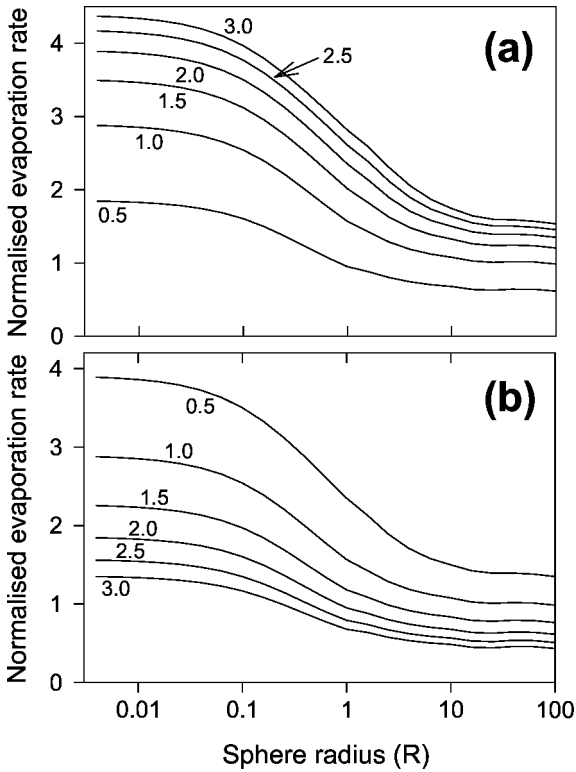

Figure 8. Effect of varying different parameters on evaporation rate for a glass-coated sphere: (a) T, and (b) Q.

The effect of sphere radius on E has been presented in Fig. 7, where it is clear that E increases with decreasing R, particularly for $R/t < 10$, i.e. the evaporation rate is larger in small R regions such as corners and points. This result appears to confirm the assumption in previous work [9] regarding the possibility of oxygen ingression at the specimen corners being due to an increased evaporation rate at this position. Therefore, it may well be the case that creep lifetime may be enhanced for specimens containing corner edges with larger values of R. This result would also indicate the necessity for continuous smooth surfaces in glass sealed CMCs. For the present case, the value of E for $R \to 0$, $E(0)$, was 2.9 times that of the flat plate value, $E(\infty)$, although it should be noted that the exact value of this ratio will depend on factors such as Q and T.

The effect of changing T and Q on E as a function of R has been presented in Figs 8a and 8b, respectively. As expected, the effect of increasing either T and decreasing Q was to increase E. The ratio of $E(0)$ to $E(\infty)$ was constant to within 5% as T and Q changed by a factor of six and thus it would appear that T and Q have negligible effect on the ratio of evaporation rates between flat and curved surfaces. On the other hand, however, the actual numerical difference between $E(0)$ and $E(\infty)$ increased significantly for increasing T and/or decreasing Q so that

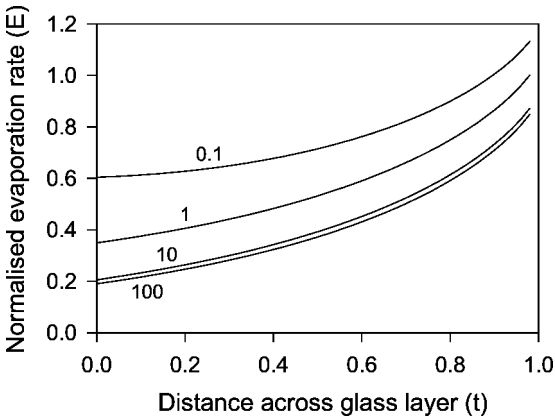

Figure 9. Effect of sphere radius on the positional dependence across the glass layer thickness to the evaporation rate.

oxygen ingression at specimen corners would be more likely to occur under these situations.

If we consider the geometry of Fig. 6, it might be useful to determine which parts of the glass layer make the largest contribution to E. Shown in Fig. 9 is the effect of changing R on the relative contribution to E from different parts of the glass layer. The first trend is that, as expected from the earlier data, contributions from each region were always higher for smaller values of R, i.e. $E\uparrow$ as $R\downarrow$. The curves for $R = 10$ and $R = 100$ were almost coincident, suggesting that, for the present calculations, an appropriate definition for what constitutes a 'corner' might be $R/t < 10$. The second trend noted is that, for each curve, values were minimum at $t = 0$ (interface between the glass and sphere) and increased to a maximum at $t = 1$ (outside surface of the glass layer). The ratio for contributions at $t = 1$ and $t = 0$ increased with increasing R, meaning that, for a flat plate, a larger proportion of the evaporation comes from close to the outer glass surface whereas for $R \to 0$ there is a larger contribution from the body of the glass layer.

Overall, it is concluded that the surface of glass-sealed materials should be as flat and smooth as possible in order to minimise differential evaporation.

4. CONCLUSIONS

In this study, results were summarised from a SEM investigation of fracture surfaces from 17 specimens of glass-sealed 3D woven SiC/SiC-based composite that had failed following creep testing at 1100 and 1200°C in air. In addition, the problem of glass evaporation from a curved surface was analysed in order to more fully understand the failure mechanism in these specimens. The SEM study concluded that nearly all specimens failed due to initial oxygen ingression at the specimen corner edges and this was attributed to a number of factors. In addition, the main pathway for oxygen movement within specimens was found to be along z fibre

bundles. Results of the analysis indicated evaporation from the glass surface layer to always be higher at curved surfaces such as corner edges when compared to flat regions.

Acknowledgements

The authors wish to sincerely thank Dr. M. Shibuya of Ube Industries Ltd., T. Hirokawa and T. Tanamura of Shikibo Ltd., and J. Gotoh of Kawasaki Heavy Industries Ltd. for their dedication in the research and development of NUSK-CMC.

REFERENCES

1. R. Naslain, Challenging ceramic matrix composites for applications in severe environments, *Adv. Composite Mater.* **5** (1), 35–44 (1995).
2. H. Hatta, T. Aoki, Y. Kogo and T. Yarii, High-temperature oxidation behavior of SiC-coated carbon fiber-reinforced carbon matrix composites, *Composites: Part A* **30**, 515–520 (1999).
3. J. B. Davis, D. B. Marshall, K. S. Oka, R. M. Housley and P. E. D. Morgan, Ceramic composites for thermal protection systems, *Composites: Part A* **30**, 483–488 (1999).
4. I. J. Davies, T. Ishikawa, M. Shibuya and T. Hirokawa, Fibre strength parameters measured in situ for ceramic matrix composites tested at elevated temperature in vacuum and air, *Compos. Sci. Technol.* **59** (6), 801–811 (1999).
5. I. J. Davies, T. Ishikawa, M. Shibuya and T. Hirokawa, Optical microscopy of 3-D woven SiC/SiC-based composites, *Compos. Sci. Technol.* **59** (3), 429–437 (1999).
6. I. J. Davies, T. Ishikawa, M. Shibuya, T. Hirokawa and J. Gotoh, Fibre and interfacial properties measured in situ for a 3-D woven SiC/SiC-based composite with glass sealant, *Composites: Part A* **30** (4), 587–591 (1999).
7. T. Ogasawara, T. Ishikawa, T. Matsuzaki, M. Suzuki, M. Shibuya, J. Gotoh and T. Hirokawa, Durability of 3-D woven Si-Ti-C-O fiber/Si-Ti-C-O matrix composite evaluated by arc jet test, *J. Ceram. Soc. Japan* **108** (1), 80–88 (2000).
8. T. Ishikawa, N. Suzuki, I. J. Davies, M. Shibuya, T. Hirokawa and J. Gotoh, Creep behavior and modeling of SiC-based PC ceramic matrix composites with glass sealing in high temperature air, *Key Eng. Mater.* **164/165**, 197–200 (1999).
9. T. Ogasawara, T. Ishikawa, N. Suzuki, I. J. Davies, M. Suzuki, J. Gotoh and T. Hirokawa, Tensile creep behavior of 3-D woven Si-Ti-C-O fiber/SiC-based matrix composite with glass sealant, *J. Mater. Sci.* **35**, 785–793 (2000).
10. M.-Y. He and J. W. Hutchinson, Crack deflection at an interface between dissimilar elastic materials, *Int. J. Solids Structures* **25** (9), 1053–1067 (1989).